Sensitive analysis on the effective soil thermal conductivity of the Thermal Response Test considering various testing times, field conditions and U-pipe lengths

Fujiao Tang, Hossein Nowamooz

Sensitive analysis on the effective soil thermal conductivity of the Thermal Response Test considering various testing times, field conditions and U-pipe lengths

Fujiao Tang & Hossein Nowamooz*

ICUBE, UMR 7357, CNRS, INSA de Strasbourg, 24 boulevard de la Victoire, 67084 Strasbourg

Highlights

- A λ ratio (= water level/U-pipe length) is defined for the Thermal Response Tests.
- The testing time, λ ratio and U-pipe length affect the Thermal Response Test results.
- The effective soil thermal conductivity varies linearly with the λ ratio.
- The soil thermal conductivity varies with the pipe length in a polynomial (2^{nd} degree) form.
- An analytical solution is proposed for the effective soil thermal conductivity.

Abstract

Thermal Response Test (TRT) is commonly conducted in geothermal projects to determine the effective ground thermal conductivity. However, the tests are hardly conducted in small or medium projects due to its considerable costs. Moreover, these projects are more likely to be influenced by the environmental conditions (climate and groundwater level) due to the shallow installation depth of the Borehole Heat Exchangers (BHEs). The objective of this investigation is to find an alternative approach for the estimation of the field effective soil thermal conductivity by considering various testing times, field conditions and U-pipe lengths. To reach this objective, a numerical framework is initially validated by the in-situ measurements. Then, it is used to simulate the TRTs conducted in clay, sandy loam and sand during the hottest day(s) of a year in summer and the coldest day(s) of a year in winter with various U-pipe lengths and groundwater levels. The results show that there is a higher effective soil thermal conductivity in winter than in summer while this difference becomes less significant for the U-pipes longer than 30 m. Among the studied soils, clay has the least effective thermal conductivity. Sandy loam shows a higher effective thermal conductivity than sand especially in the short U-pipes. The effective soil thermal conductivity varies linearly with a newly defined λ ratio (the water level depth divided by the U-pipe length). It also varies with the U-pipe length in a polynomial form (2^{nd} degree). Finally, an analytical approach is proposed to estimate the effective soil thermal conductivity. The approach is validated by 6 in-situ measurements. The capacity of the approach is also evaluated by a regional multi-layered field.

Keywords

Analytical approach; Borehole Heat Exchanger; Effective soil thermal conductivity; Field condition; Testing time; Thermal Response Test; U-pipe length.

Nomenclature

		u	velocity, $m.s^{-1}$
A	U-pipe cross-sectional area, m^2	x_s	sand content
C_p	specific heat capacity, $J.kg^{-1}.K^{-1}$	z	depth beneath land surface, m
C_v	volumetric heat capacity, $J.m^{-3}.K^{-1}$	z_u	depth of unsaturated zone, m
d_h	U-pipe inner diameter, m	$z_{U\text{-}pipe}$	U-pipe length, m
f_D	Darcy friction factor		
H_p	water potential or suction head, m	*Greek symbols*	
K	hydraulic conductivity, $m.s^{-1}$	α	independent parameter, m^{-1}
k	thermal conductivity, $W.m^{-1}.K^{-1}$	γ_d	soil dry unit weights, $kN.m^{-3}$
l	pore connectivity parameter	γ_s	soil specific unit weights, $kN.m^{-3}$
L	borehole length, m	ε	difference, %
m	index	θ	volumetric water content
n	independent parameter	ρ	density, $kg.m^{-3}$
q	heat extraction rate, $W. m^{-1}$		
Q	energy source, $W.m^{-3}$	*Subscripts*	
Q_p	energy source in pipe flow, $W.m^{-1}$	b	borehole
r	distance between borehole center and surrounding medium, m	eff	effective
R_b	borehole thermal resistance, $K.m.W^{-1}$	f	fluid
S_e	relative saturation	inlet	inlet node of U-pipe
S_r	saturation of soil	outlet	outlet node of U-pipe
t	time, s	res	residual
T	temperature, °C	s	soil
T_0	initial temperature, °C	sat	saturated

1 Introduction

Geothermal energy is clean, efficient, sustainable [1], and can be accessed all over the world. Ground Source Heat Pump (GSHP) is a traditional approach to exploit geothermal energy, and Thermal Response Test (TRT) is popularly conducted during the design stage of a GSHP to mainly decide the effective ground thermal conductivity and the borehole thermal resistance. TRT has firstly been proposed by Mogensen in 1983 [2]. The first mobile measurement devices are introduced in Sweden [3] and then in the USA [4]. Since then, the test approach has spread rapidly and is available in about 40 countries worldwide [5,6].

In a conventional TRT, a constant power input is applied to soil with a continuous water flow during 2 or 3 days [7,8], and the inlet/outlet fluid temperatures are continuously measured to determine bulk thermal properties over the borehole length [9,10].

Although the fiber-optic Distributed Temperature Sensing (DTS) [11,12] is available now to characterize the vertical thermophysical properties, the traditional TRT has not lost its popularity. The TRT provides an average depth of the ground, indicating that the ground heterogeneity and anisotropy can be ignored [13]. Fig. 1 shows a TRT performed in a multi-layered field and its corresponding effective thermal conductivity. By comparing two models with homogeneous and stratified subsurface layers, Luo et al. [14] found that there was no significant difference between the fluid outlet temperatures in both models. After conducting the in-situ experiments for a heterogeneous rock, Radioti et al. [13] employed the measured effective ground thermal conductivity in their numerical framework and concluded that the bedrock heterogeneity was not critical in the Borehole Heat Exchanger (BHE) simulations. Claesson and Eskilson [15] found also that the temperatures in the heat extraction mode were not different in homogeneous and stratified grounds.

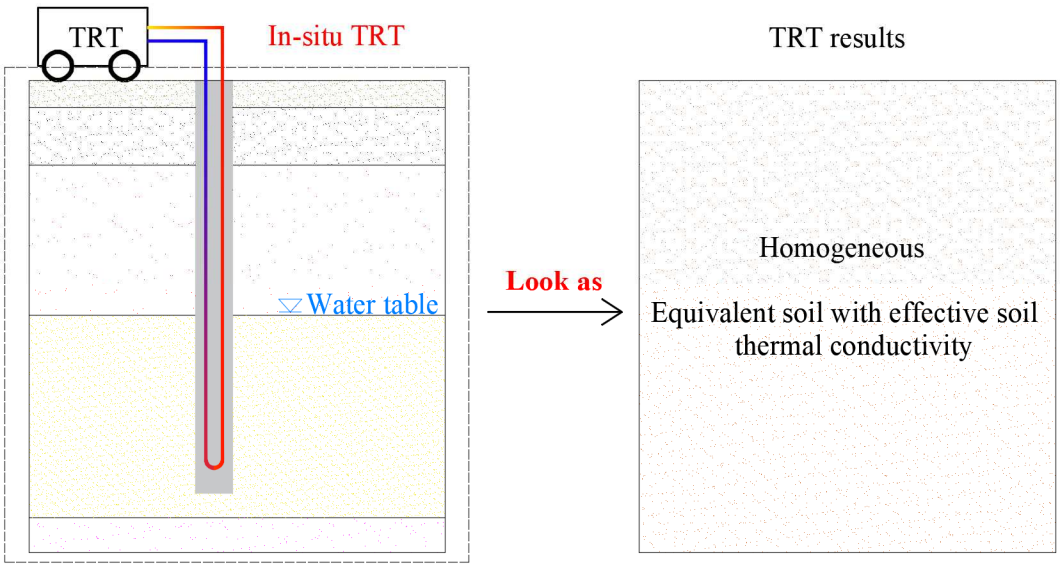

Fig. 1 Schematic diagram for TRT and test results.

The traditional method to analyze the TRT results is the Infinite Line Source Model (ILSM) [16], and the ground temperature variation (ΔT) at a given time (t) and distance (r) can be expressed as:

$$\begin{aligned}\Delta T = T(r,t) - T_0 &= -\frac{q}{4\pi k_s} Ei\left(-\frac{C_{v-s} r^2}{4 k_s t}\right) \\ &= -\frac{q}{4\pi k_s}\left(0.5772 + \ln\frac{C_{v-s} r^2}{4 k_s t} - \sum_{m=1}^{\infty} \frac{(-1)^{m-1} \cdot C_{v-s} r^2 / (4 k_s t)}{m \cdot m!}\right)\end{aligned} \tag{1}$$

where, T_0 is initial ground temperature (°C), Ei is the integral exponential function, q is the heat per unit length of the line heat source ($W.m^{-1}$), k_s is the soil thermal conductivity ($W.m^{-1}.K^{-1}$), C_{v-s} is the soil volumetric heat capacity ($J.m^{-3}.K^{-1}$), m is the index number, and 0.5772 is the Euler constant. When t is sufficiently large and $C_{v-s}r^2/(4k_st)$ is sufficiently small (less than 0.05) [17], the above equation can be approximated as:

$$\Delta T = T(r,t) - T_0 = \frac{q}{4\pi k_s}\ln(t) - \frac{q}{4\pi k_s}\left(\ln\frac{C_{v-s} r^2}{4 k_s} + 0.5772\right) \tag{2}$$

The borehole thermal resistance can be defined as:

$$R_b = \frac{\overline{T}_f - T(r_b,t)}{q} \tag{3}$$

where, r_b is the borehole radius (m).

Therefore, the average fluid temperature can be obtained:

$$\overline{T}_f = T(r_b,t) + qR_b = \frac{q}{4\pi k_s}\ln(t) - \frac{q}{4\pi k_s}\left(\ln\frac{C_{v-s} r_b^2}{4 k_s} + 0.5772\right) + qR_b + T_0 \tag{4}$$

where, the average fluid temperature is conventionally defined as the mean value of the carrying fluid inlet and outlet temperature ($(T_{inlet}+T_{outlet})/2$). In the right part of the above equation, only the first term is variable with time and the other terms remain constant.

Therefore, the effective soil thermal conductivity can be estimated after the stabilization of the fluid temperature with the natural logarithm of time:

$$k_s = \frac{q}{4\pi} \cdot \frac{\Delta \ln(t)}{\Delta \overline{T}_f} \tag{5}$$

Due to the simplicity and reliability of ILSM, it has been adopted into many investigations. Lee et al. [18] used the method to analyze the TRT results of an in-situ Standing Column Well (SCW) geothermal heat exchanger. Luo et al. [19] applied the method to 17 in-situ TRTs with specific configurations and ground conditions in Wuhan (China). Radioti et al. [13] used ILSM to get the effective ground thermal conductivity of 4 sites on the campus of the University of Liege (Belgium). Zhou et al. [20] used ILSM to analyze in-situ TRTs conducted in Donghua University (China). Spitler et al. [21] conducted 5 TRTs on the campus of Chalmers University of Technology (Sweden) and ILSM was used to estimate the thermal resistance of groundwater-filled boreholes in both heat extraction and injection modes.

Groundwater level affects the effective soil thermal conductivity obtained from the TRTs. The groundwater level divides the soil into saturated and unsaturated zones. The saturated zone has normally a higher soil thermal conductivity. In the unsaturated zone, the soil thermal conductivity is largely dependent on field geology and suction/water content profiles [22,23]. Luo et al. [24] conducted six TRTs at two sites in a loess deposit with different groundwater levels and they found that the effective ground thermal conductivity increased remarkably with the increase of groundwater level, indicating that the effective thermal conductivity of the ground increased from 1.64 $W.m^{-1}.K^{-1}$ to 2.07 $W.m^{-1}.K^{-1}$ when the groundwater level changed from 35 m to 10 m. By conducting TRTs for a BHE in a karstic aquifer field, Smith et al. [25] identified the significant influence of the water table on the effectiveness of the system. They suggested that TRTs should be conducted multiple times to better characterize

the saturated zone.

In practice, the annual temperature fluctuation on the land surface influences the ground temperature up to 10 m below land surface [26]. Thus, seasonal land surface hydrothermal fluctuation also influences the TRT results [27].

Few studies have considered the variations of water level and seasonal temperature on the TRT [28] and further studies are still necessary for the seasonal climate changes in shallow depths. In this context, a Finite Element Method (FEM) is adopted to simulate the TRT during the hottest day(s) of a year in summer and during the coldest day(s) of a year in winter. The investigated soils are constituted of unsaturated and saturated zones, where the thermal properties in the saturated zone are constant and the soil thermal properties in the unsaturated zone are decided by the soil hydraulic profile.

Another objective of this study is to find an alternative approach to estimate the effective soil thermal conductivity since TRT is not conducted in some small or medium projects due to its relatively high capital investment. For example, a TRT for a borehole with a depth between 100 and 120 m can cost between 3000 and 5000 £ in England [29]. In these cases, the ground thermal conductivity normally relies on the known results of TRTs performed in nearby locations [30]. By analyzing the different cases in the numerical simulations, a new analytical approach is also proposed for the estimation of the effective soil thermal conductivity in BHE allpications.

2 Governing equations of the numerical framework

A FEM is employed in this paper to simulate TRTs. The same numerical framework has been used in our previous papers [26,31]. The principal equations of this framework are summarized in Table 1. Although there is a small impact of Darcy friction and heat

conduction of carrying fluid on the current TRT results (less than 0.5%), they are also taken into account in equation (12) by respecting the energy balance equation.

Table 1 Governing equations of the numerical framework [26]

Physics	Governing equation *
	$S_e = \begin{cases} \dfrac{1}{\left[1+\left\|\alpha H_p\right\|^n\right]^{1-1/n}} & H_p < 0 \\ 1 & H_p \geq 0 \end{cases}$ (6)
Hydrothermal fluctuation in soil (used for deriving initial soil hydrothermal profiles)	$\theta = S_e \cdot (\theta_{sat} - \theta_{res}) + \theta_{res}$ (7)
	$S_r = \theta / \theta_{sat}$ (8)
	$k_s = (0.443x_s + 0.081\gamma_d)\dfrac{(4.4x_s + 0.4)S_r}{1+(4.4x_s - 0.6)S_r} + 0.087x_s + 0.019\gamma_d$ (9)
	$C_{v-s} = (4.18 - 0.095\gamma_d - 0.3x_s)S_r + 0.09\gamma_d - 0.2x_s$ (10)
Energy balance in soil	$\rho_s C_{p-s}\dfrac{\partial T_s}{\partial t} = k_s \nabla \cdot (\nabla T_s) + Q_s$ (11)
Energy balance in pipe	$A\rho_f C_{p-f}\dfrac{\partial T_f}{\partial t} + A\rho_f C_{p-f}\mathbf{u}_f \cdot \nabla T_f = \nabla \cdot Ak_f \nabla T_f + f_D \dfrac{\rho_f A}{2d_h}\mathbf{u}_f\mathbf{u}_f^2 + Q_p$ (12)

*S_e: relative saturation; α: independent parameter, m^{-1}; H_p: water potential or suction head, m; n: independent parameter; θ: volumetric water content; θ_{sat}: saturated volumetric water content; θ_{res}: residual volumetric water content; S_r: saturation of soil; x_s: sand content; γ_d: soil dry unit weights, $kN.m^{-3}$; C_{v-s}: soil volumetric heat capacity, $J.m^{-3}.K^{-1}$; ρ_s: soil density, $kg.m^{-3}$; C_{p-s}: soil specific heat capacity, $J.kg^{-1}.K^{-1}$; T_s: soil temperature, °C; t: time, s; Q_s: soil energy source, $W.m^{-3}$; A: U-pipe cross-sectional area, m^2; ρ_f: carrying fluid density, $kg.m^{-3}$; C_{p-f}: carrying fluid specific heat capacity, $J.kg^{-1}.K^{-1}$; T_f: carrying fluid temperature, °C; u_f: velocity, $m.s^{-1}$; f_D: Darcy friction factor; d_h: U-pipe inner diameter, m; Q_p: energy source in pipe flow, $W.m^{-1}$.

3 Validation of the numerical framework for the TRTs

In-situ TRTs conducted at the Chiba Experimental Station at the University of Tokyo (Japan) [32] are used to evaluate the capacity of the numerical framework. The water level is situated at a depth of 10 m and the U-pipe length is 50 m. The effective soil thermal conductivity of 1.96 $W.m^{-1}.K^{-1}$ is employed in the model [32]. All the site parameters are reported in Table 2.

Table 2 Input parameters of the simulated in-situ TRT in Tokyo (Japan) [27,32]

Parameter, unit	Value
Carrying fluid density, $kg.m^{-3}$	1000
Carrying fluid specific heat capacity, $J.kg^{-1}.K^{-1}$	4200
Carrying fluid thermal conductivity, $W.m^{-1}.K^{-1}$	0.6
Carrying fluid velocity, $m.s^{-1}$	0.53
U-pipe type, -	Single

U-pipe thickness, m	0.0034
U-pipe inner diameter, m	0.0270
U-pipe heat conductivity, $W.m^{-1}.K^{-1}$	0.38
Borehole diameter, m	0.165
Grout heat conductivity, $W.m^{-1}.K^{-1}$	1.43 [27]
Grout volumetric heat capacity, $MJ.m^{-3}.K^{-1}$	1.9 [32]
Shank spacing, m	0.05
Effective soil thermal conductivity, $W.m^{-1}.K^{-1}$	1.96
Soil volumetric heat capacity, $MJ.m^{-3}.K^{-1}$	2.5
Initial temperature, °C	17
Operation time, h	72
Outlet temperature – inlet temperature, °C	1.673

Fig. 2 shows the comparison between the in-situ measurements and the model predictions of the inlet/outlet fluid temperatures. The difference between the measurements and the predictions is presented by ε, given as:

$$\varepsilon = \frac{\left| T_{numerical} - T_{in-situ} \right|}{T_{numerical}} \times 100\% \tag{13}$$

The comparisons show that the numerical framework is capable to predict well the inlet and outlet temperatures, particularly after 20 h. The difference is relatively large in the first 20 h. After this time, the difference becomes less than 1%.

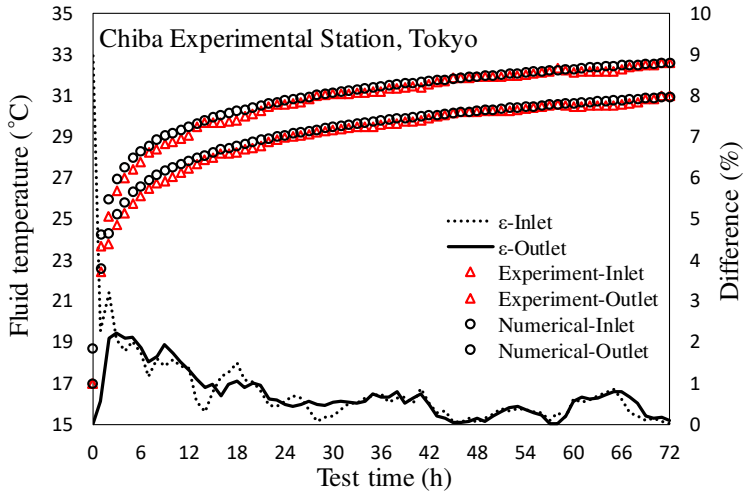

Fig. 2 Comparison between the in-situ measurements and the numerical simulations: the fluid inlet/outlet temperatures and their differences (ε).

However, the concept of TRTs is based on a homogenized one-layered soil but the ground is often stratified, and the thermal conductivity is then a function of depth: k = k (z). We use the following equation to obtain the equivalent thermal conductivity:

$$k = \frac{1}{L}\int_{z}^{z+L} k(z)dz \tag{14}$$

where, L is the length of the BHE (m), z is the starting depth where the BHE is installed (m).

To further evaluate the capacity of our proposed numerical framework, TRTs are simulated for a BHE installed in Alsace region (France) [26] since we have access to an instrumented site in this region. Alsace has a semi-continental climate at low altitude and a continental climate at high altitude. At some parts of the region, the ground temperature gradient can reach 0.1 °C.m^{-1}. The lowest daily average ambient temperature at the test site is around 1 °C in winter and the highest daily average ambient temperature in summer is around 22 °C. The annual average ambient temperature at the test site is around 11.5 °C. Table 3 presents 6 different soil layers and their thicknesses. The U-pipe is surrounded by grout and water is the carrying fluid. Further details about the field, the weather condition, the grout thermal properties, the U-pipe description, the physical properties of the carrying fluid and the U-pipe layout are given in our previous publication [26].

Table 3 Six soil layers with their thicknesses at a site in Alsace region (France)

Soil layer	Soil category	Thickness (m)
1	Clay loam	0.1
2	Sandy loam 1	1.0
3	Loam	0.15
4	Sandy loam 1	4.75
5	Sandy loam 2	8.0
6	Loam	11.0

By using equation (14), the equivalent soil thermal conductivities are then obtained 1.659 and 1.662 W.m^{-1}.K^{-1} respectively in summer and winter. The heat injection rate is 60 W.m^{-1}. Fig. 3

shows the comparison of the average fluid temperatures of the TRTs conducted in summer and winter for the stratified and its equivalent soil. It shows that the effect of the heterogeneity is not significant in our numerical approach and the equivalent thermal conductivity can provide correctly the effective thermal conductivity.

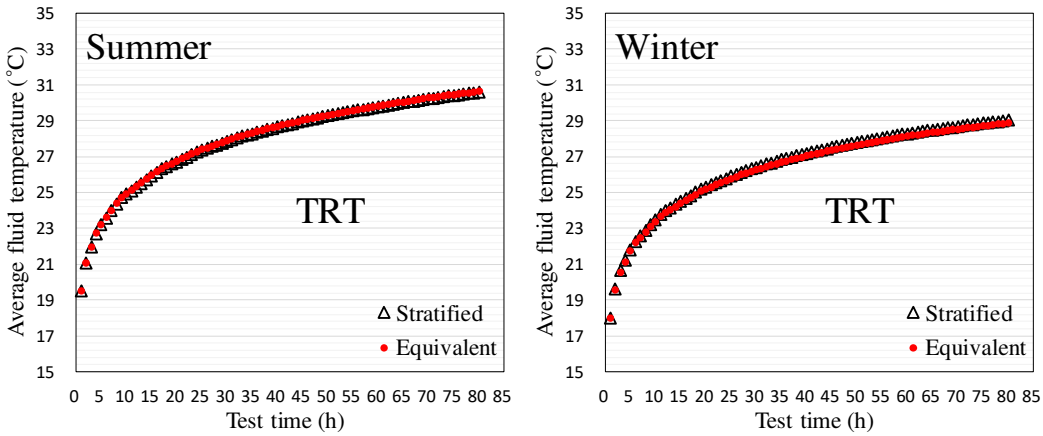

(a) (b)

Fig. 3 Comparison of the average carrying fluid temperatures for the stratified field and its equivalent soil in two seasons conducting TRTs: (a) summer and (b) winter.

4 TRT simulation results

In this section, the simulation results of the TRTs conducted in different scenarios are presented.

4.1 Model description

A 3D geometry with a length of 30 m, a width of 30 m and a depth of 100 m is used in the numerical simulations. The borehole diameter is 0.14 m. Inside the borehole, the single U-tube is symmetrically positioned with a shank spacing of 0.05 m. The inner and outer diameters of U-pipe are respectively 2.2 and 2.7 cm.

In practice, a BHE is conventionally surrounded by unsaturated and saturated soils, and the depth of the unsaturated zone varies with the water level. The soil thermal properties vary with time and space, particularly in the unsaturated zone. To better investigate the influence of

this unsaturated zone on the effective soil thermal conductivity, a λ ratio is introduced:

$$\lambda = \frac{z_u}{z_{U-pipe}} \tag{15}$$

where, z_u is the depth of unsaturated zone/water level (m), $z_{U\text{-}pipe}$ denotes the U-pipe length (m). In the investigation, the λ ratio ranges between 0 to 1, indicating that the unsaturated zone does not exceed the U-pipe length.

To have a more comprehensive investigation, 10 scenarios are considered by modifying either the U-pipe length or the water level. In this work, the U-pipe length is between 11.5 and 34.03 m, the water level is between 8.45 and 15 m and the λ ratio is between 0.34 and 1. Table 4 summarizes these scenarios with their corresponding λ ratios.

Table 4 Summary of the 10 scenarios for 6 U-pipe lengths and 3 water levels

Scenario	U-pipe length $z_{U\text{-}pipe}$ (m)	Water level z_u (m)	$\lambda=z_u/z_{U\text{-}pipe}$
S1	15	8.45	0.56
S2		11.5	0.77
S3		15.0	1
S4	20.42	11.5	0.56
S5	11.5		1
S6	25	8.45	0.34
S7		11.5	0.46
S8		15.0	0.6
S9	34.03	11.5	0.34
S10	19.17		0.6

It is expected that the effective ground thermal conductivity ranges between a value obtained during the hottest day(s) of a year and a value obtained during the coldest day(s) of a year. Hot days of a year are supposed to be in summer and cold days of a year are in winter. Thus, summer and winter express these extreme conditions in our simulations. The daily average land surface temperatures for the hottest day(s) in summer and the coldest day(s) in winter are respectively considered 25 and 0 °C. The temperature profiles on the hottest and the coldest days are also presented in Fig. 4-a.

To explore the influence of the water level on the TRT, three water levels of 8.45 m, 11.5 m and 15.0 m are used for the different scenarios as mentioned in Table 4. The suction profiles of these 3 water levels in summer and winter are then presented in Fig. 4 b-d.

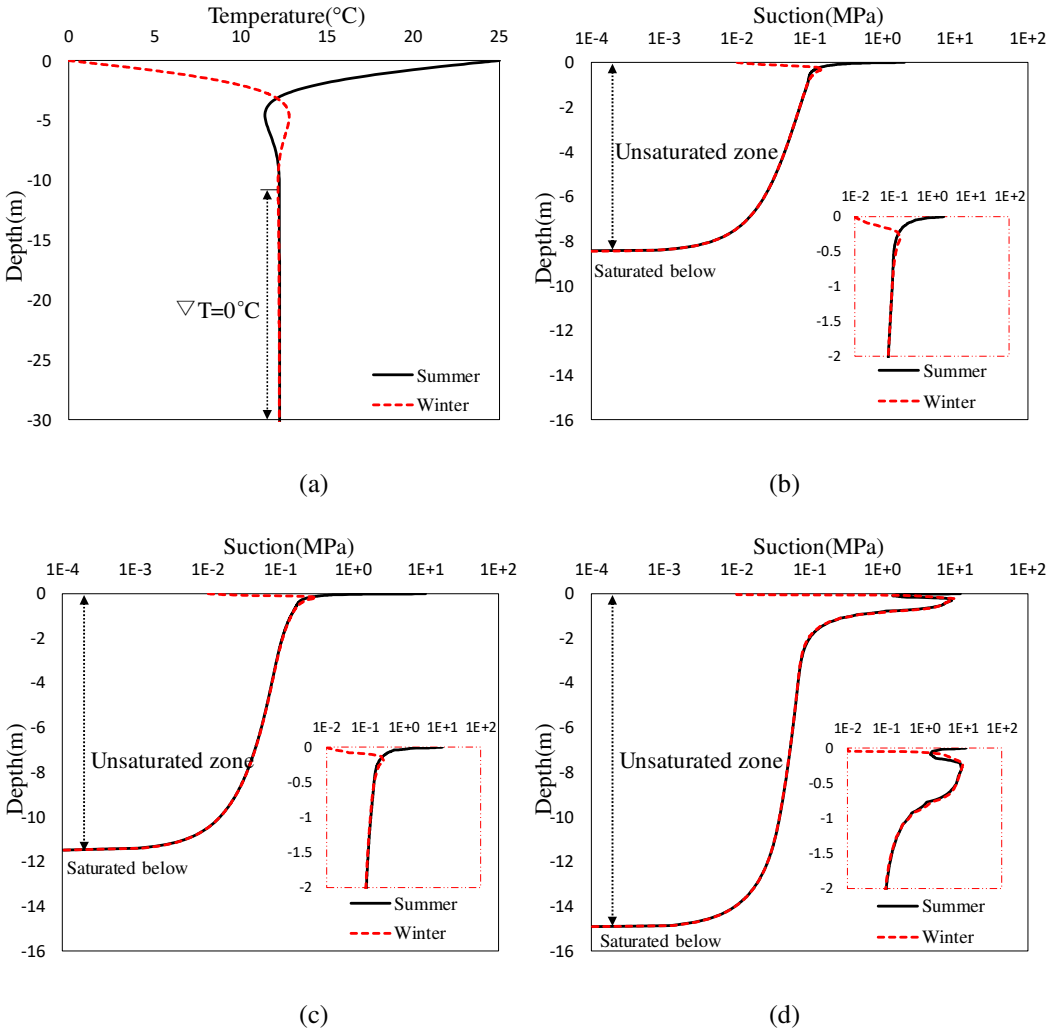

Fig. 4 Initial hydrothermal profiles of the model for 2 seasons (winter & summer): (a) ground temperature; (b) suction profiles in scenarios S1 and S6; (c) suction profiles in scenarios S2, S4, S5, S7, S9 and S10; and (d) suction profiles in scenarios S3 and S8.

The sand content is used in this work to represent the different field conditions since it affects directly the soil thermal properties in the numerical framework (equations (9) and (10)). Three typical soils with 20%, 60% and 90% of sand content, representing clay, sandy loam and sand are adopted to investigate the TRTs in the different geotechnical (field) conditions. Table 5

summaries the hydrothermal parameters necessary in equations (6) to (10) and their corresponding values for the 3 soils. The soil specific unit weights (γ_s) are also presented.

Table 5 Hydrothermal properties of the studied soils

Soil	γ_d (kN.m^{-3})	x_s (-)	K (m.s^{-1})	l (-)	α (m^{-1})	n (-)	θ_{sat} (-)	θ_{res} (-)	γ_s (kN.m^{-3})
Clay	14.2	0.2	1.44E-6	0.5	1.98	1.086	0.481	0.010	27.4
Sandy loam	16.1	0.6	4.42E-6	0.5	2.49	1.170	0.392	0.010	26.4
Sand	16.1	0.9	1.03E-4	0.5	4.30	1.520	0.366	0.025	25.4

The water retention curves and their corresponding soil thermal properties obtained from equations (9) and (10) for the studied soils are presented in Fig. 5. The variation of these thermal properties is presented with the degree of saturation (Fig. 5-b & c). As it is known, soil is conventionally made up of mineral particles (represented by sand content in this study), water and air. Water (with a thermal conductivity of 0.6 W.m^{-1}.K^{-1}) has a higher thermal conductivity than air (with a thermal conductivity of 0.026 W.m^{-1}.K^{-1}) and it acts as bridges to connect mineral particles together. The higher the water content, the higher the soil thermal conductivity (Fig. 5-b). A higher sand content results in a higher thermal conductivity (Fig. 5-b). The volumetric heat capacity decreases inversely with the increase of the sand content (Fig. 5-c).

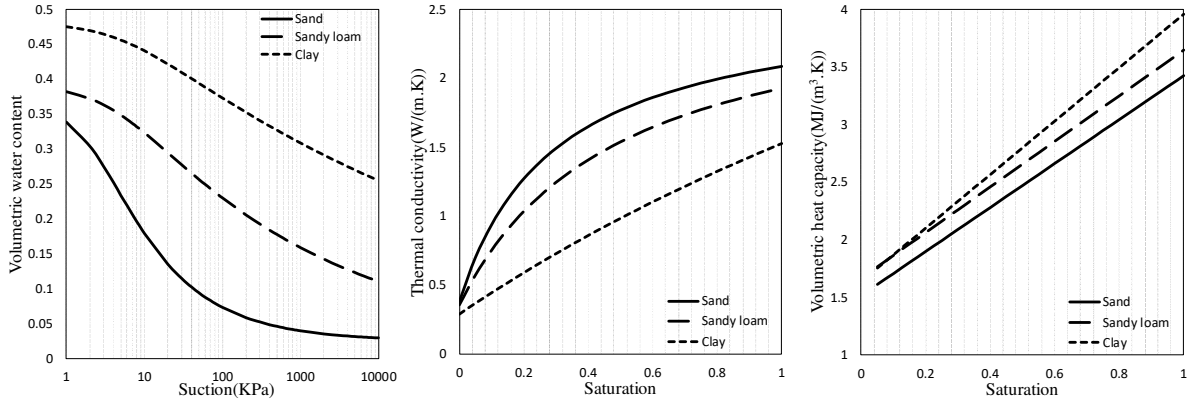

(a) (b) (c)

Fig. 5 Hydrothermal properties of the 3 soils: (a) water retention curves; (b) thermal conductivity and (c)

volumetric heat capacity.

By using the equations (9) and (10), and the initial suction profiles (presented in Fig. 4), the initial soil thermal properties can be obtained. Fig. 6 shows the initial thermal properties of the 3 soils at the water level of 8.45 m (scenarios S1 and S6) in summer and winter. In general, clay has the lowest thermal conductivity. Sand has the highest thermal conductivity in the saturated zone while sandy loam has the highest thermal conductivity in the unsaturated zone. Furthermore, clay has the highest volumetric heat capacity.

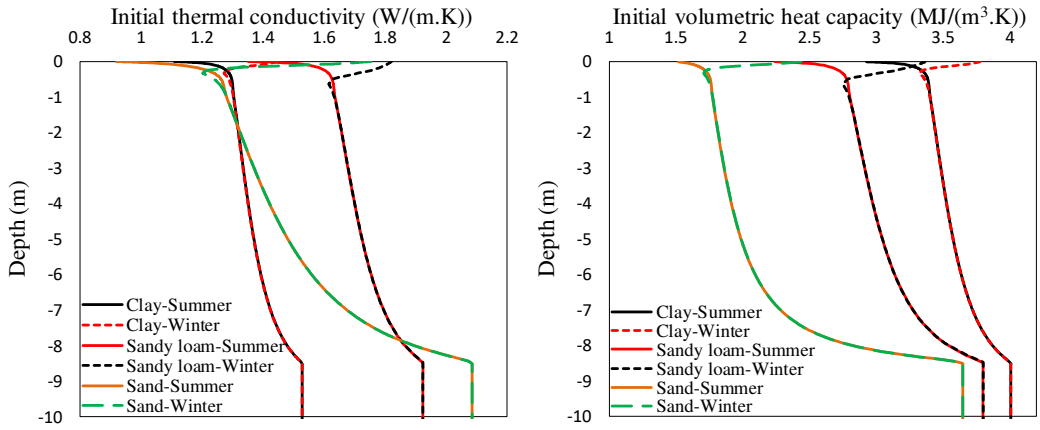

(a) (b)

Fig. 6 Initial thermal properties of the studied soils for a water level of 8.45 m (scenarios S1 and S6) in summer and winter: (a) thermal conductivity and (b) volumetric heat capacity.

Water is selected as the circulating fluid in the U-pipe with the velocity of 0.5 $m.s^{-1}$. The thermal conductivity of pipe is 0.5 $W.m^{-1}.K^{-1}$. The grout has a thermal conductivity of 2.5 $W.m^{-1}.K^{-1}$, a density of 2500 $kg.m^{-3}$ and a specific heat capacity of 800 $J.kg^{-1}.K^{-1}$.

Due to a limited hydraulic velocity in clay and the water head difference in shallow BHEs, no groundwater flow is imposed in the numerical simulations.

Conventional TRTs usually need a time between 48 and 72 hours [7,8]. Consequently, a period of 120 h is considered in our simulations to cover sufficiently this period.

The heat injection process is only considered in our investigation, which is common in the

TRT practice. ASHRAE standards recommend a thermal load between 50 and 80 $W.m^{-1}$ for a TRT [33,34]. Cai et al. [35] have experimentally conducted TRTs subjected to 3 heat loads and found that the heating power influenced less than 5% the ground thermal conductivity. Accordingly, a heat injection rate of 60 $W.m^{-1}$ is chosen for the following TRT simulations.

4.2 Numerical simulation results for carrying fluid temperature

The carrying fluid temperatures are obtained for the 10 scenarios in clay, sandy loam and sand in summer and winter. Fig. 7 shows the variation of the mean carrying fluid temperature with the natural logarithm of time for clay and sand in summer and winter where Su, Wi, Cl and Sa stand respectively for summer, winter, clay and sand. The figure shows that the fluid temperature increases with time due to the heat accumulation in soil. Moreover, the fluid temperature is higher in summer than in winter, mainly due to a higher land surface temperature in summer. The fluid temperature of BHE installed in sand has a larger range of variation. The fluid temperature increases with the λ ratio in summer for all the studied soils. However, it decreases with the increase of λ ratio for some cases in clay and in winter: S4-Wi-Cl, S5-Wi-Cl, S9-Wi-Cl and S10-Wi-Cl. The carrying fluid temperature in sand also increases with the λ ratio in all the scenarios. Since the TRT results in sandy loam show the same tendency observed in clay, these results are not presented in Fig. 7. In the next section, these results will be considered.

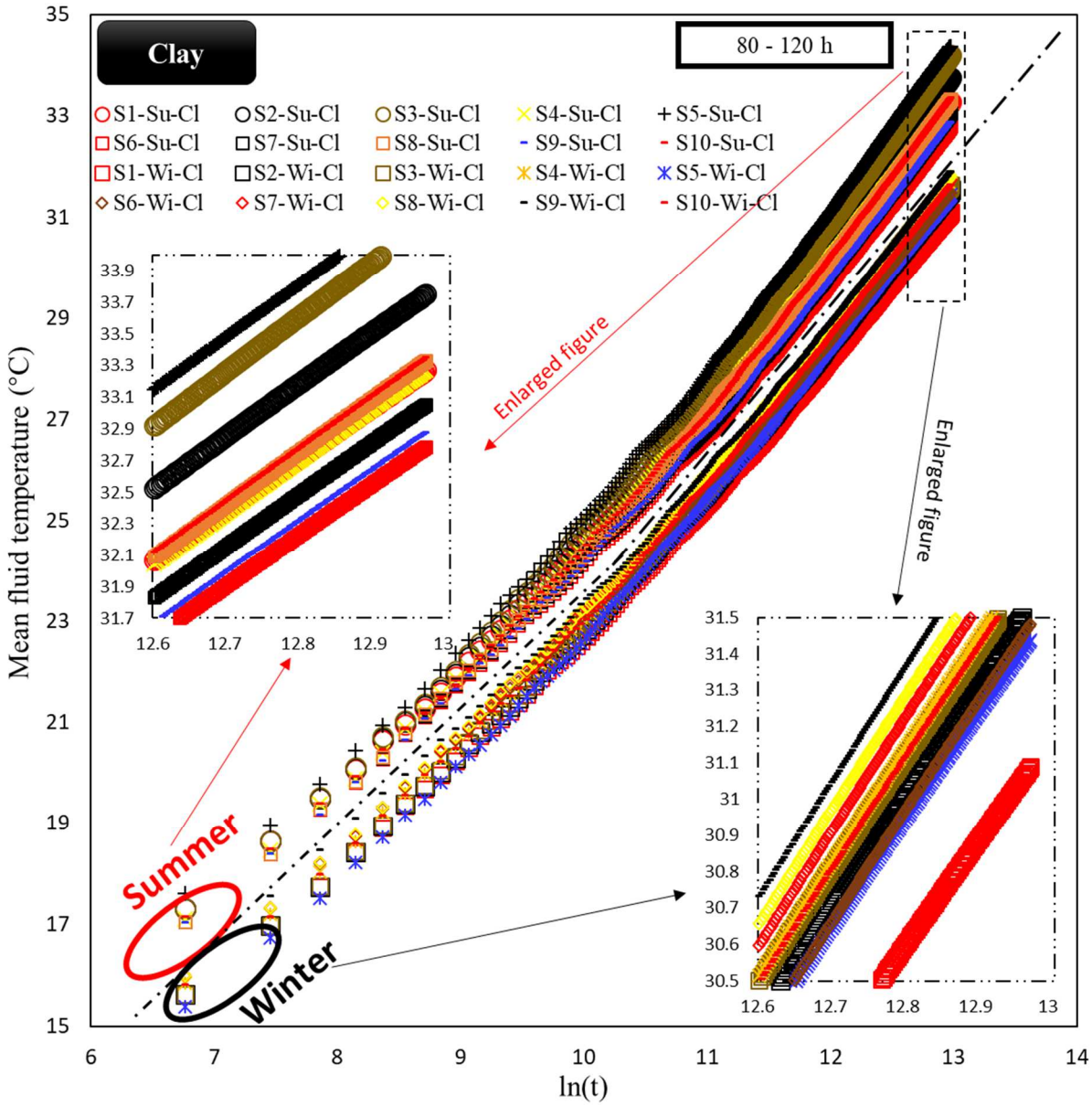
Clay
80 - 120 h
S1-Su-Cl
S2-Su-Cl
S3-Su-Cl
S4-Su-Cl
S5-Su-Cl
S6-Su-Cl
S7-Su-Cl
S8-Su-Cl
S9-Su-Cl
S10-Su-Cl
S1-Wi-Cl
S2-Wi-Cl
S3-Wi-Cl
S4-Wi-Cl
S5-Wi-Cl
S6-Wi-Cl
S7-Wi-Cl
S8-Wi-Cl
S9-Wi-Cl
S10-Wi-Cl
Enlarged figure
Enlarged figure
Summer
Winter
Mean fluid temperature (°C)
ln(t)

(a)

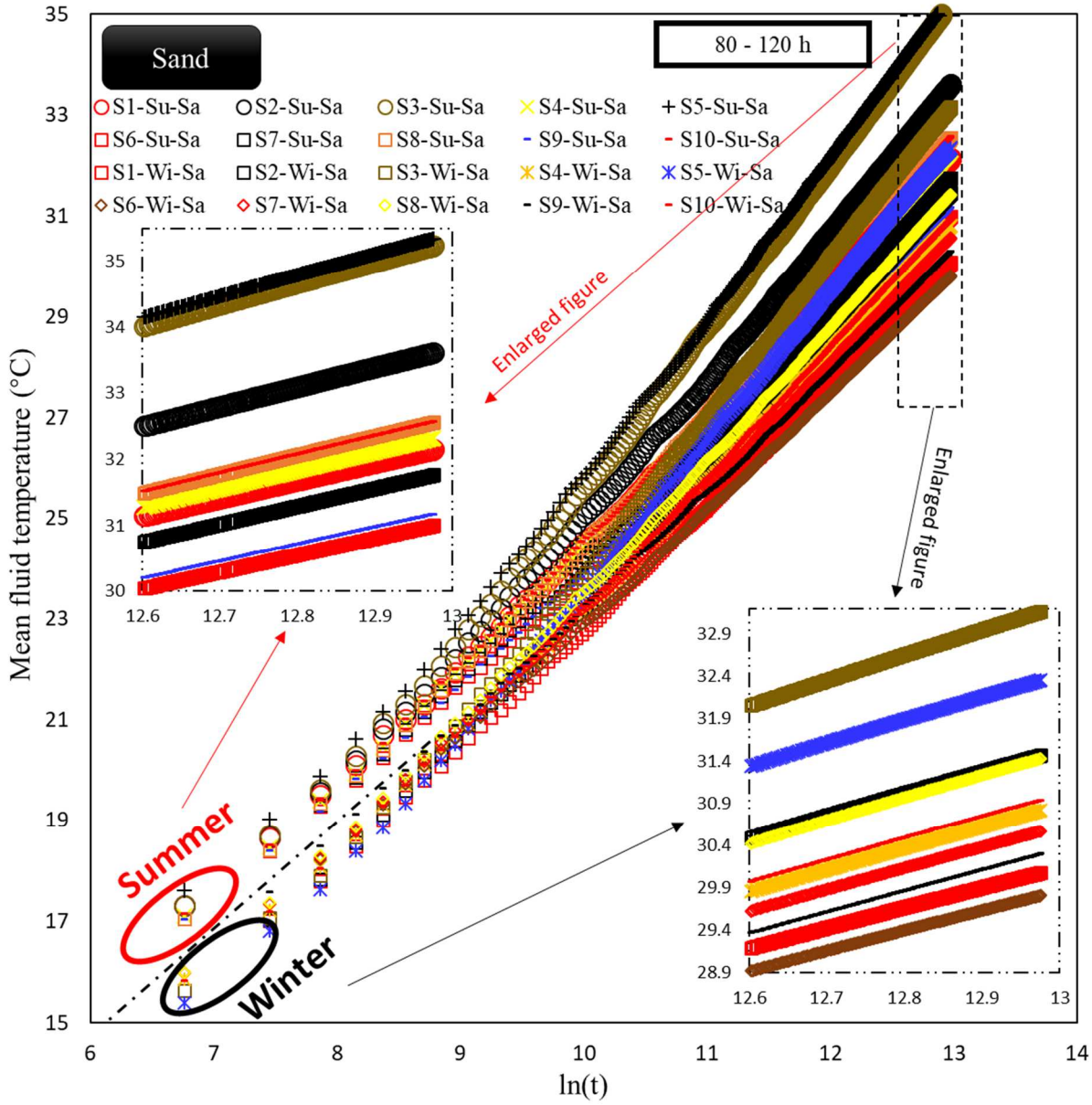

(b)

Fig. 7 Mean carrying fluid temperature from TRTs in summer and winter for different soils: (a) clay and (b) sand.

4.3 Numerical simulation results for the effective soil thermal conductivity

The testing time, the soil, the λ ratio and the U-pipe length influence the fluid temperature, and consequently the effective soil thermal conductivity. The fluid temperature between 80 and 120 h are eventually chosen to acquire the effective soil thermal conductivity by using equation (5), since the TRT reaches a steady state in this stage.

To better analyze the TRT results and explore the effect of λ ratio and U-pipe length on the results, the tests are divided into 2 groups as presented in Table 6.

Table 6 Two proposed groups for a more comprehensive analysis of the TRTs

Group	Scenario	Water table (m)	U-pipe length (m)
1	S1, S2, S3, S6, S7, S8	Variable	15 & 25 (Constant)
2	S2, S4, S5, S7, S9, S10	11.5 (Constant)	Variable

Fig. 8 shows the variation of the effective thermal conductivity of clay, sandy loam and sand with the λ ratio and the U-pipe length in summer and winter for the two groups. The results of the second group are presented with both λ ratio and U-pipe length.

The figure shows that the effective soil thermal conductivities obtained in winter are higher than those in summer (3.8% to 14.0% for clay, 5.8% to 24.3% for sandy loam, and 5.2% to 17.9% for sand), and the largest difference exists for the shortest U-pipe. The phenomenon is due to a favorable heat transfer during the heat injection period in winter.

The figure also shows that the effective soil thermal conductivity varies linearly with the λ ratio (Fig. 8 a-f) and it additionally varies in a (2^{nd} degree) polynomial form with the U-pipe length (Fig. 8 g-i).

Generally, clay has the smallest effective thermal conductivity among the 3 soils. Sand and sandy loam have a larger variation of the effective thermal conductivities than clay. Further, sandy loam has a greater effective thermal conductivity than sand in shallow U-pipes. The phenomenon can be explained by Fig. 6-a, where sandy loam has a higher thermal conductivity in its unsaturated zone. However, the advantage would diminish with the increase of the U-pipe length, since sand has a higher thermal conductivity in the saturated zone.

In Group 1 with a variable water level, the decrease of the effective soil thermal conductivity

with the λ ratio is observed for all the soils (Fig. 8 a-c). In Group 2 with a variable U-pipe length, the same trend is observed for clay and sandy loam in summer while an increase of their effective thermal conductivity occurs during winter (Fig. 8-d & e). Fig. 8-f illustrates that the effective soil thermal conductivity of sand decreases with the λ ratio in summer and winter.

Moreover, the difference between the effective thermal conductivity in summer and winter decreases with the increase of U-pipe length, and the decrease rate is stabilized for the lengths longer than 30 m (Fig. 8 g-i). It means that the testing time affects less the TRT results in long U-pipes.

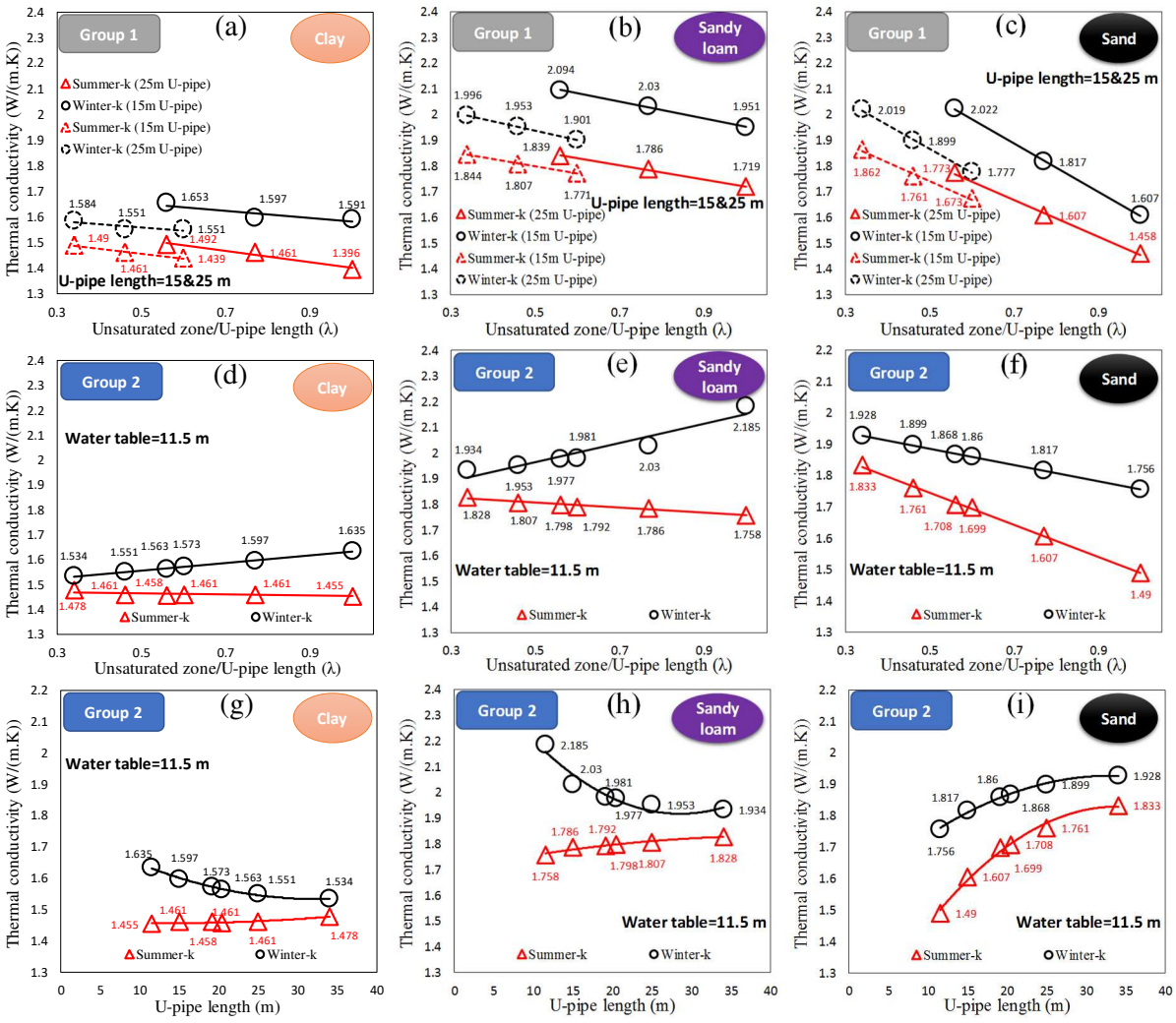

Fig. 8 Effective soil thermal conductivity variation of the 3 soils in summer and winter for group 1 with the λ

ratio (a to c) and for group 2 with the λ ratio (d to f) and the U-pipe length (g to i).

5. An analytical approach for the effective soil thermal conductivity and its applications

In this section, an analytical approach is first proposed and then applied to 6 in-situ measurements and a geothermal multi-layered field in Alsace region (France).

5.1 The proposed analytical approach

It has been obtained in the last section that the soil effective thermal conductivity varies linearly with the λ ratio (Fig. 8 a-f) and it varies with the U-pipe length in a polynomial form (Fig. 8 g-i). Fig. 8 g-i also show that the effective soil thermal conductivity is stabilized for the long U-pipes. This maximum U-pipe length in which the stabilization occurs is noted as L_{max} (m).

According to the results in the last section, the following solution is proposed to predict the effective soil thermal conductivity:

$$k_{eff} = \begin{cases} a + b \cdot \lambda + c \cdot \chi^2 + d \cdot \chi & (\chi < 1) \\ e + b \cdot \lambda & (\chi \geq 1) \end{cases} \quad (16)$$

where a ($W.m^{-1}.K^{-1}$), b ($W.m^{-1}.K^{-1}$), c ($W.m^{-1}.K^{-1}$), d ($W.m^{-1}.K^{-1}$) and e ($W.m^{-1}.K^{-1}$) are constant parameters. The λ ratio varies between 0 and 1. χ is another dimensionless factor, defined as:

$$\chi = \frac{z_{U-pipe}}{L_{max}} \quad (17)$$

By fitting the results, all the parameters estimated in the two seasons for the 3 soils are summarized in Table 7. The table indicates that the proposed equation (16) considers

indirectly the soil saturation, its dry density, and its sand content since the coefficients vary with the soil type and the season. It also confirms that the λ ratio define reasonably the effect of the unsaturated zone on the effective thermal conductivity.

Table 7 Fitted parameters of the proposed analytical solution (equation (16)) for the 3 soils in summer and winter

Soil	Season	a ($W.m^{-1}.K^{-1}$)	b ($W.m^{-1}.K^{-1}$)	c ($W.m^{-1}.K^{-1}$)	d ($W.m^{-1}.K^{-1}$)	e ($W.m^{-1}.K^{-1}$)	L_{max} (m)
Clay	Summer	1.810	-0.2092	0.26134	-0.52295	1.549	30.6
	Winter	2.060	-0.1936	0.45347	-0.90740	1.606	34.9
Sandy loam	Summer	2.178	-0.273	0.25685	-0.51449	1.920	31.7
	Winter	3.028	-0.312	0.98515	-1.96840	2.045	30.4
Sand	Summer	2.354	-0.7261	0.29137	-0.58208	2.07	41.4
	Winter	3.154	-0.9278	0.90042	-1.80194	2.252	34.5

As the sand content is the unique instinctive parameter distinguishing the three studied soils in this work, the relation between the fitted parameters with the sand content are also presented in Fig. 9. The figure shows that 3 parameters (a, b and e) increase/decrease constantly with the sand content. However, the other parameters (c, d and L_{max}) do not follow a continuous trend (decrease or increase) with the sand content, which is due to the climate changes in shallow depths. When the U-pipe length is beyond L_{max}, the corresponding parameters (b and e) increase/decrease constantly with the sand content.

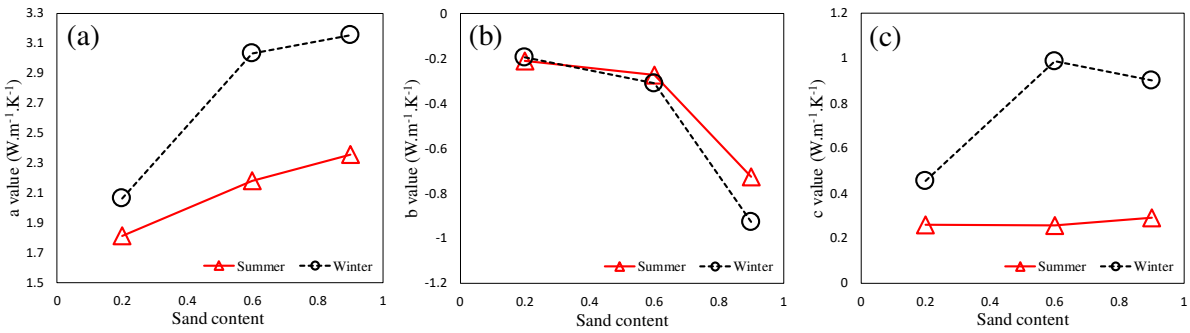

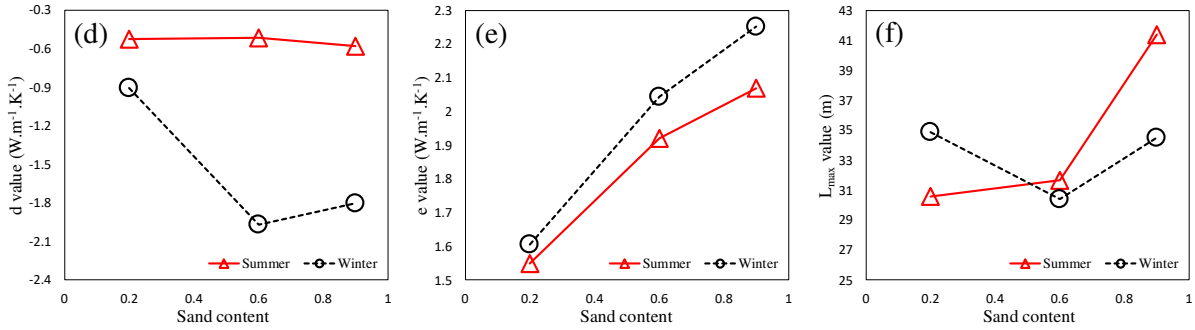

Fig. 9 Variation of the fitted parameters for the proposed approach with the sand content in summer and winter: (a) parameter a; (b) parameter b; (c) parameter c; (d) parameter d; (e) parameter e and (f) parameter L_{max}.

The fitted curves of the proposed approach and the TRT simulation results are additionally shown in the 3D (effective thermal conductivity - λ ratio - U-pipe length) plane, presented in Fig. 10. The results show that the proposed approach predicts well the effective soil thermal conductivities with RMSE values less than 0.035 $W.m^{-1}.K^{-1}$.

The L_{max} values varying between 30 and 42 m confirm also the necessity of the proposed analytical solutions since the traditional TRTs are normally conducted for BHEs beyond 50 m and these TRTs are independent of the U-pipe length based on our calculations.

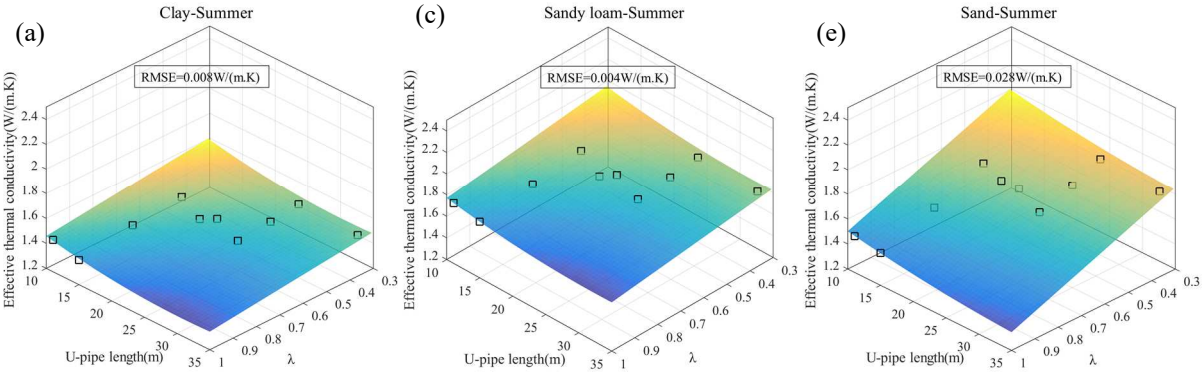

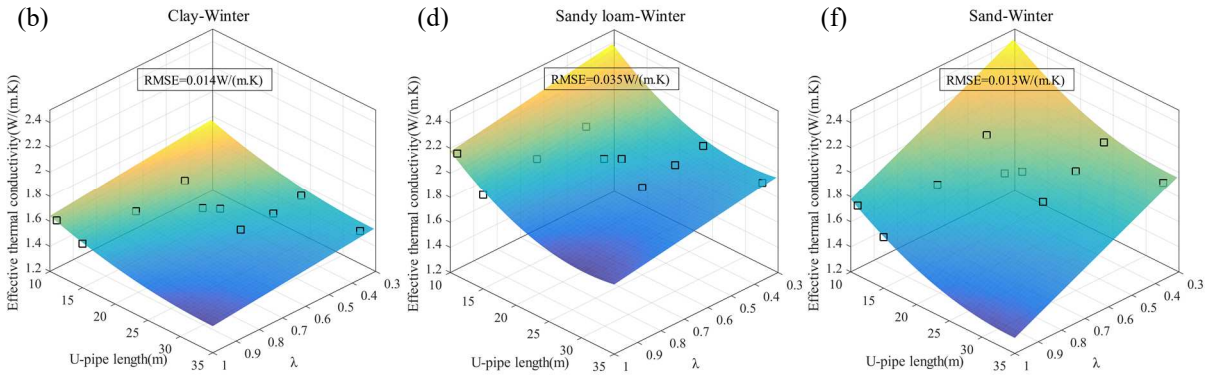

Fig. 10 Fitted curves and the simulation results in the (effective thermal conductivity - λ ratio - U-pipe length) plane: (a) clay in summer; (b) clay in winter; (c) sandy loam in summer; (d) sandy loam in winter; (e) sand in summer and (f) sand in winter.

5.2 The application of the proposed approach to the in-situ measurements

The approach has been used to predict the effective soil thermal conductivity of 6 sites all around the world. As observed in Fig. 8 g-i, the effective soil thermal conductivity is less influenced by the testing time (winter or summer) when the U-pipe length exceeds L_{max}. Since all these studies have a U-pipe length longer than 50 m, it is not necessary to estimate two different thermal conductivities in summer and winter as the difference will be less than 5.5%. Therefore, an average value of the effective soil thermal conductivity in summer and winter is estimated for the three soils (Table 8). The measured in-situ effective soil thermal conductivities are also reported in Table 8. The results show that the in-situ soil thermal conductivities for the 6 sites are between the smallest (clay k_{eff}) and the largest (sand k_{eff}) values, proving the capacity of the proposed approach.

The proposed approach can be also used to approximate the geotechnical field condition by comparing the in-situ thermal conductivity with the predicted values for the different soils. For example, it can be declared that the Japanese soil in Choi and Ooka's work [32] has a geotechnical texture between sand and sandy loam and the Cyprian soil in Florides and Kalogirou's work [38] has more or less a clayey texture.

Table 8 Comparison of the measured and predicted effective soil thermal conductivities (k_{eff}) for the 6 sites

Source	Country	z_u (m)	$z_{U\text{-}pipe}$ (m)	Predicted k_{eff} ($W.m^{-1}.K^{-1}$)			In-situ k_{eff} ($W.m^{-1}.K^{-1}$)
				Clay	Sandy loam	Sand	
Choi and Ooka [32]	Japan	10	50	1.54	1.92	2.00	1.96
Saito et al. [36,37]	Japan	11	50	1.53	1.92	1.98	1.71
Luo et al. [24]	China	35	120	1.52	1.90	1.92	1.64
Luo et al. [24]	China	10	120	1.56	1.96	2.09	2.07
Florides and Kalogirou [38]	Cyprus	15	50	1.52	1.89	1.91	1.61
Soldo et al. [39]	Croatia	15	100	1.55	1.94	2.04	1.92

5.3 The application of the proposed approach to a multi-layered field in Alsace (France)

To further verify the capacity of the proposed approach, TRTs are also simulated in Alsace region (France) for a BHE with a U-pipe length of 20 m and a water level of 7.63 m (presented in section 3). The U-pipe has also penetrated through 6 soil layers (Table 3).

The validity of an equivalent one-layered soil in the TRT numerical simulations was confirmed in section 3. Fig. 3 compared the average carrying fluid temperatures of a one-layered equivalent soil with a multi-layered soil for TRTs conducted in summer and winter and for a period of 80 hours.

Fig. 11 shows additionally the average carrying fluid temperatures of the one-layered equivalent soil with the natural logarithm of time to deduce the effective soil thermal conductivity. The derived effective soil thermal conductivities range between 1.71 $W.m^{-1}.K^{-1}$ in summer and 1.79 $W.m^{-1}.K^{-1}$ in winter. The effective thermal conductivity is rationally higher in winter than in summer. The effective soil thermal conductivities of the different studied soils in summer and winter are also reported in Fig. 11 as the reference values. The obtained effective soil thermal conductivities are close to the equivalent thermal conductivity derived from equation (14): 1.659 $W.m^{-1}.K^{-1}$ in summer and 1.662 $W.m^{-1}.K^{-1}$ in winter (presented in section 3). These facts give more credits to the proposed approach for the

estimation of the effective soil thermal conductivity in a shallow BHE.

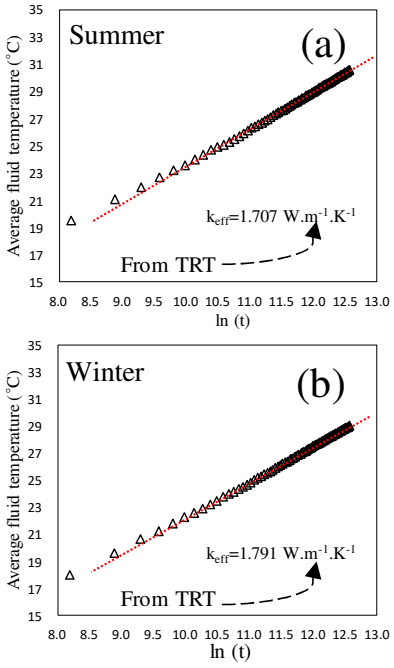

Summer

Prediction model	k_{eff} (W.m^{-1}.K^{-1})
Clay	1.50
Sandy loam	1.85
Sand	1.82

Winter

Prediction model	k_{eff} (W.m^{-1}.K^{-1})
Clay	1.59
Sandy loam	2.04
Sand	2.01

Fig. 11. Comparison of the effective soil thermal conductivity from the numerical simulation and the analytical approach for a multi-layered soil in Alsace region (France), in (a) summer and (b) winter.

6 Conclusion

In this investigation, the impacts of testing time, field condition and U-pipe length on TRTs have been studied. Eventually, an analytical approach has been proposed to estimate the effective soil thermal conductivity in BHE applications.

Generally, the TRT numerical simulations are conducted in 3 soils, 2 seasons, 3 water levels and 6 U-pipe lengths. In total, 60 cases are simulated, and their corresponding effective soil thermal properties are obtained. The results show that the TRTs in winter have higher effective soil thermal conductivities, due to the heat injection process. The influence of the testing time becomes less significant as the U-pipe length increases. The effective soil thermal conductivity varies linearly with the λ ratio (= water level/ U-pipe length) and it decreases generally with the increase of the λ ratio in summer. On the contrary, it increases with the λ ratio for the tests in clay and sandy loam with a constant water level during winter. Moreover,

the effective thermal conductivity varies with the U-pipe length in a (2^{nd} degree) polynomial form, and the influence of U-pipe length on effective soil thermal conductivity generally gets stabilized when the U-pipe is beyond 30 m.

By analyzing the TRT results, an analytical solution is proposed to estimate the effective soil thermal conductivity, with a RMSE less than 0.035 $W.m^{-1}.K^{-1}$. The approach has been used to estimate the effective soil thermal conductivities of 6 sites in Japan, China, Cyprus and Croatia, along with a shallow BHE installed in a multi-layered field in Alsace region (France). The comparisons prove the good capacity of the proposed approach to estimate the field effective thermal conductivities in the BHE projects with various field conditions and U-pipe lengths. The proposed approach is particularly interesting for short BHEs with limited capital investments.

Acknowledgment

The China Scholarship Council (CSC) has supported this work.

References

[1] Atam E, Helsen L. Ground-coupled heat pumps: Part 2-Literature review and research challenges in optimal design. Renew. Sustain. Energy Rev. 2016; 54: 1668-1684. http://dx.doi.org/10.1016/j.rser.2015.07.009.

[2] Mogensen P. Fluid to duct wall heat transfer in duct system heat storage. In: Proceedings of the International Conference on Surface Heat Storage in Theory and Practice. Stockholm (Sweden); 1983; 652-657.

[3] Eklof C, Gehlin S. TED-a mobile equipment for thermal response tests. M.S. Thesis. Lulea University of Technology (Sweden); 1996.

[4] Austin W.A. Development of an in situ system for measuring ground thermal properties. M.S. Thesis. Oklahoma State University (USA); 1998.

[5] Nordell B. Thermal response test (TRT)—state of the art 2011. Report from IEA ECES ANNEX 21, 2011.

[6] Spitler J, Gehlin S. Thermal response testing for ground source heat pump systems-an historical review. Renew. Sustain. Energy Rev. 2015; 50:1125-37. https://doi.org/10.1016/j.rser.2015.05.061.

[7] Bujok P, Grycz G, Klempa M, Kunz A, Porzer M, Pytlik A, Rozehnal Z, Vojcinák P. Assessment of the influence of shortening the duration of TRT (thermal response test) on the precision of measured values. Energy 2014. 64: 120-129. https://doi.org/10.1016/j.energy.2013.11.079.

[8] Raymond J, Lamarche L, Malo M. Extending thermal response test assessments with inverse numerical modeling of temperature profiles measured in ground heat exchangers. Renewable Energy 2016. 99: 614-621. https://doi.org/10.1016/j.renene.2016.07.005.

[9] Raymond J, Therrien R, Gosselin L, Lefebvre R. A review of thermal response test analysis using pumping test concepts. Ground Water 2011; 49:932-45. https://doi.org/10.1111/j.1745-6584.2010.00791.x.

[10] Angelotti A, Ly F, Zille A. On the applicability of the moving line source theory to thermal response test under groundwater flow: considerations from real case studies. Geothermal Energy 2018; 6:12. https://doi.org/10.1186/s40517-018-0098-z.

[11] Fujii H, Okubo H, Nishi K, Itoi R, Ohyama K, Shibata K. An improved thermal response test for U-tube ground heat exchanger based on optical fiber thermometers. Geothermics 2009; 38 399-406. https://doi.org/10.1016/j.geothermics.2009.06.002.

[12] Beier R, Acuña J, Mogensen P, Palm B. Vertical temperature profiles and borehole resistance in a U-tube borehole heat exchanger. Geothermics 2012; 44: 23-32. https://doi.org/10.1016/j.geothermics.2012.06.001.

[13] Radioti G, Cerfontaine B, Charlier R, Nguyen F. Experimental and numerical investigation of a long-duration Thermal Response Test: Borehole Heat Exchanger behaviour and thermal plume in the heterogeneous rock mass. Geothermics 2018. 71: 245-258. https://doi.org/10.1016/j.geothermics.2017.10.001.

[14] Luo J, Rohn J, Bayer M, Priess A, Xiang W. Analysis on performance of borehole heat exchanger in a layered subsurface. Applied Energy 2014; 123:55-65. https://doi.org/10.1016/j.apenergy.2014.02.044.

[15] Claesson J, Eskilson P. Conductive heat extraction to a deep borehole: thermal analyses and dimensioning rules. Energy 1988. 13: 509-527. https://doi.org/10.1016/0360-5442(88)90005-9.

[16] Carslaw HS, Jaeger JC. Conduction of Heat in Solids second ed. Oxford University

Press: Oxford (UK); 1959.
[17] Brunetti G, Saito H, Saito T, Šimůnek J. A computationally efficient pseudo-3D model for the numerical analysis of borehole heat exchangers. Applied Energy 2017; 208: 1113-1127. https://doi.org/10.1016/j.apenergy.2017.09.042.
[18] Lee C, You J, Park H. In-situ response test of various borehole depths and heat injection rates at standing column well geothermal heat exchanger systems. Energy & Buildings 2018; 172 201-208. https://doi.org/10.1016/j.enbuild.2018.05.009.
[19] Luo J, Luo Z, Xie J, Xia D, Huang W, Shao H, Xiang W, Rohn J. Investigation of shallow geothermal potentials for different types of ground source heat pump systems (GSHP) of Wuhan city in China. Renewable Energy 2018; 118: 230-244. https://doi.org/10.1016/j.renene.2017.11.017.
[20] Zhou Y, Zhao L, Wang S. Determination and analysis of parameters for an in-situ thermal response test. Energy and Buildings 2017; 149: 151-159. https://doi.org/10.1016/j.enbuild.2017.05.048.
[21] Spitler J, Javed S, Ramstad. Natural convection in groundwater-filled boreholes used as ground heat exchangers. Applied Energy 2016; 164: 352-365. https://doi.org/10.1016/j.apenergy.2015.11.041.
[22] Nowamooz H, Nikoosokhan S, Lin J, Chazallon C. Finite difference modeling of heat distribution in multilayer soils with time-spatial hydrothermal properties. Renewable Energy 2015; 76: 7-15. https://doi.org/10.1016/j.renene.2014.11.008.
[23] Tang F, Nowamooz H. Hydro-Thermal Properties of the Unsaturated Soil. Conference: Civil Infrastructures Confronting Severe Weathers and Climate Changes Conference. Hangzhou, China; 2018. doi: 10.1007/978-3-319-95744-9_2.
[24] Luo J, Tuo J, Huang W, Zhu Y, Jiao Y, Xiang W, Rohn J. Influence of groundwater levels on effective thermal conductivity of the ground and heat transfer rate of borehole heat exchangers. Applied Thermal Engineering 2018; 128: 508-516. https://doi.org/10.1016/j.applthermaleng.2017.08.148.
[25] Smith D, Elmore A, Thompson J. The effect of seasonal groundwater saturation on the effectiveness of large scale borehole heat exchangers in a karstic aquifer. Geothermics 2018; 75: 164-170. https://doi.org/10.1016/j.geothermics.2018.05.001.
[26] Tang F, Nowamooz H. Long-term performance of a shallow borehole heat exchanger installed in a geothermal field of Alsace region. Renewable Energy 2018; 128: 210-222. https://doi.org/10.1016/j.renene.2018.05.073.

[27] Choi W, Ooka R. Effect of disturbance on thermal response test, part 2: Numerical study of applicability and limitation of infinite line source model for in-terpretation under disturbance from outdoor environment. Renewable Energy 2016; 85: 1090-1105. http://dx.doi.org/10.1016/j.renene.2015.07.049.

[28] Jensen-Page L, Narsilio G, Bidarmaghz A, Johnston I. Investigation of the effect of seasonal variation in ground temperature on thermal response tests. Renewable Energy 2018; 125: 609-619. https://doi.org/10.1016/j.renene.2017.12.095.

[29] Synergy. Geological Survey/ TRT/ Design. 2018. < http://www.synergyboreholes.co.uk/geothermal_boreholes/index/trt/> [accessed 27.06.18].

[30] Mikhaylova O, Johnston I, Narsilio G. Uncertainties in the design of ground heat exchangers. Environmental Geotechnics 2016; 3:253-264. https://doi.org/10.1680/jenge.15.00033.

[31] Tang F, Nowamooz H. Factors influencing the performance of shallow Borehole Heat Exchanger. Energy Conversion and Management 2019; 181:571-583. https://doi.org/10.1016/j.enconman.2018.12.044.

[32] Choi W, Ooka R. Effect of natural convection on thermal response test conducted in saturated porous formation: Comparison of gravel-backfilled and cement-grouted borehole heat exchangers. Renewable Energy 2016; 96: 891-903. https://doi.org/10.1016/j.renene.2016.05.040.

[33] ASHRAE Handbook - HVAC Applications, Chapter 34 Geothermal Energy, 2011.

[34] Zhang C, Song W, Sun S, Peng D. Parameter estimation of in-situ thermal response test with unstable heat rate. Energy 2015; 88: 497-505. https://doi.org/10.1016/j.energy.2015.05.074.

[35] Cai Y, Xu H, Chen S. Testing and analysis of the influence factors for the ground thermal parameters. Applied Thermal Engineering 2016; 107: 662-671. https://doi.org/10.1016/j.applthermaleng.2016.06.186.

[36] Saito T, Hamamoto S, Mon E. E, Takemura T, Saito H, Komatsu T, Moldrup P. Thermal properties of boring core samples from the Kanto area, Japan: Development of predictive models for thermal conductivity and diffusivity. Soils and Foundations 2014; 54: 116-125. https://doi.org/10.1016/j.sandf.2014.02.004.

[37] Saito T, Hamamoto S, Ueki T, Ohkubo S, Moldrup P, Kawamoto K, Komatsu T. Temperature change affected groundwater quality in a confined marine aquifer during long-term heating and cooling. Water Research 2016; 94: 120-127.

https://doi.org/10.1016/j.watres.2016.01.043.
[38] Florides G, Kalogirou S. First in situ determination of the thermal performance of a U-pipe borehole heat exchanger, in Cyprus. Applied Thermal Engineering 2008; 28: 157-163. https://doi.org/10.1016/j.applthermaleng.2007.03.026.
[39] Soldo V, Borovic S, Leposa L, Boban L. Comparison of different methods for ground thermal properties determination in a clastic sedimentary environment. Geothermics 2016; 61: 1-11. https://doi.org/10.1016/j.geothermics.2015.12.010.